NANO LETTERS

Letter

pubs.acs.org/NanoLett

Manipulating Thermal Conductance at Metal–Graphene Contacts via Chemical Functionalization

Patrick E. Hopkins,*[,†] Mira Baraket,[§] Edward V. Barnat,[‡] Thomas E. Beechem,[‡] Sean P. Kearney,[‡] John C. Duda,[†,‡] Jeremy T. Robinson,[∥] and Scott G. Walton*[,§]

[†]Department of Mechanical and Aerospace Engineering, University of Virginia, Charlottesville, Virginia 22904-4746, United States

[‡]Sandia National Laboratories, Albuquerque, New Mexico 87185, United States

[§]Plasma Physics Division, and [∥]Electronics Science and Technology Division, Naval Research Laboratory, Washington, DC 20375, United States

ABSTRACT: Graphene-based devices have garnered tremendous attention due to the unique physical properties arising from this purely two-dimensional carbon sheet leading to tremendous efficiency in the transport of thermal carriers (i.e., phonons). However, it is necessary for this two-dimensional material to be able to efficiently transport heat into the surrounding 3D device architecture in order to fully capitalize on its intrinsic transport capabilities. Therefore, the thermal boundary conductance at graphene interfaces is a critical parameter in the realization of graphene electronics and thermal solutions. In this work, we examine the role of chemical functionalization on the thermal boundary conductance across metal/graphene interfaces. Specifically, we metalize graphene that has been plasma functionalized and then measure the thermal boundary conductance at Al/graphene/SiO_2 contacts with time domain thermoreflectance. The addition of adsorbates to the graphene surfaces are shown to influence the cross plane thermal conductance; this behavior is attributed to changes in the bonding between the metal and the graphene, as both the phonon flux and the vibrational mismatch between the materials are each subject to the interfacial bond strength. These results demonstrate plasma-based functionalization of graphene surfaces is a viable approach to manipulate the thermal boundary conductance.

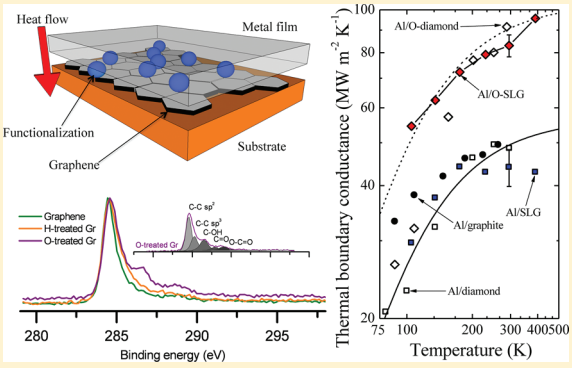

KEYWORDS: *Graphene, thermal boundary conductance, chemical functionalization, adsorbates, bond strength, Raman spectroscopy, X-ray photoelectron spectroscopy, time domain thermoreflectance, sp^3 bonding*

Graphene-based devices have garnered tremendous attention due to the unique physical properties arising from this purely two-dimensional carbon sheet.[1,2] These unique properties allow for tremendous efficiency in the transport of not only charge carriers but thermal carriers (i.e., phonons) as well.[3−7] For these reasons, graphene is being pursued both for a variety of electronic applications and as an enabler of next-generation thermal solutions. As such, it is necessary for this two-dimensional material to be able to efficiently transport heat into the surrounding 3D device architecture in order to fully capitalize on its intrinsic transport capabilities. Therefore, efficient heat flow across solid-graphene interfaces as described by the thermal boundary conductance,[8] or Kapitza conductance,[9] h_K, is vital for the realization of graphene electronics and thermal solutions.

To this end, previous groups have measured h_K at SiO_2/graphene (ref 10) and Au/graphene/SiO_2 interfaces (ref 4). The SiO_2/graphene interface exhibited a thermal boundary conductance at room temperature of ∼90 MW m^{-2} K^{-1} (ref 11). In contrast, the Au-graphene interface demonstrated a thermal boundary conductance at room temperature that was nearly a factor of 2 lower (refs 4 and 12). This discrepancy can be explained utilizing traditional phonon scattering models (e.g., diffuse mismatch model, or DMM[13]) in which the lower conductance at the Au boundary is attributed to this material having a lower energy cutoff of available modes available to transport energy as compared to both the graphene and SiO_2. While this theory is supported in part by investigations of metal/graphite interfaces, chemical bonding between the layers has been shown to play a prominent role in phonon transmission and thus h_K as well.[14] In spite of this fact, the interplay between chemical bonding, the allowable phonon modes, and the subsequent effect on interfacial thermal transport remains unclear. For graphene boundaries, meanwhile, the material's inherent surface sensitivity will only enhance this interplay.

In response, we investigate the role of interfacial bonding at metal/single-layer-graphene (SLG) interfaces by introducing chemical adsorbates on the SLG surfaces in order to increase

Received: September 2, 2011
Revised: November 14, 2011
Published: January 3, 2012

   dx.doi.org/10.1021/nl203060j | *Nano Lett.* 2012, 12, 590–595

the density of covalent bonds bridging the metal and the SLG. In doing so, we demonstrate plasma-based functionalization of graphene surfaces as a means to manipulate the thermal boundary conductance. Specifically, we metalize plasma-functionalized graphene and then measure h_K at Al/SLG/SiO_2 contacts with time domain thermoreflectance (TDTR).[15,16] From these measurements, adsorbates on the SLG surfaces are shown to influence the cross plane thermal conductance. This is attributed to changes in the bonding between the metal and the SLG. Additionally, the Al/SLG/SiO_2 thermal boundary conductance is shown to consist of two individual conductances, Al/SLG and SLG/SiO_2, in line with the conclusions from ref 4. Using our measured values of h_K in conjunction with previous measurements between metals and carbon-based materials,[4,14] the thermal boundary conductance is found to be most influenced by the interfacial chemical bonding as both the phonon flux and the vibrational mismatch between the materials are each subject to the interfacial bond strength.

The graphene films were grown by chemical vapor deposition on Cu substrates and transferred to SiO_2/Si substrates using the conventional wet chemical approach.[17] The graphene films were then functionalized with either oxygen or hydrogen using electron beam generated plasmas[18] produced in gas mixtures containing O_2 and H_2, respectively. Electron beam generated plasmas are particularly attractive in that they offer high plasma densities (10^{10}–10^{11} cm^{-3}) along with low electron temperatures (<1 eV), which provides large fluxes of low energy (<5 eV) ions[19] thereby eliminating ion-induced etching or sputtering of the basal plane. For this work, the process parameters include a pressure of 50 mTorr Ar diluted with either O_2 or H_2, where the reactive gas was 5% of the total flow rate. The plasma was operated at a duty factor of 10% (2 ms pulse width and 20 ms period) and the total treatment time was 60 s (plasma exposure time was 6 s.). The functionalization process leads to an inclusion of chemical moieties on the graphene surface, which was verified by X-ray photoelectron spectroscopy (XPS). The total oxygen present on the surface after treatment in the oxygen containing plasma is ~25 at.%. A careful inspection of the C1s peak reveals the presence of hydroxyl and carboxyl groups as indicated by the well-pronounced peaks around 286.6 and 289 eV (Figure 1a). Although the presence of hydrogen cannot be quantified by XPS, the broadening of the main peak (located at 384.5 eV) indicates the increase of sp^3 hybridized carbon atoms, which is mainly attributed to the incorporation of hydrogen. From the fitting procedure, the contribution from the sp^3 peak (situated at +0.65 eV from main peak) increased from 22% for graphene to ~33% for H-treated graphene (Figure 1a).

To structurally characterize the graphene films, we perform Raman spectroscopy on the functionalized samples along with a reference film. In each case, a Raman spectrum is acquired every 333 nm across a 15 × 15 μm area using 532 nm laser light resulting in a data set of 2025 spectra for each sample. Laser powers were not found to damage the sample. Using the fwhm of 2D mode at ~2678 cm^{-1}, each of the films are found to be composed almost completely of SLG.[20] As very little difference in the character of the graphene is found across the sample, each of the SLG spectra are averaged and shown in Figure 1b.

Before functionalization, the graphene films contain very little disorder as the ratio of the D-band (~1350 cm^{-1}) intensity to that of the G-band (~1580 cm^{-1}) is $I(D)/I(G) \approx 0.2$. Significant levels of disorder become apparent, however, upon

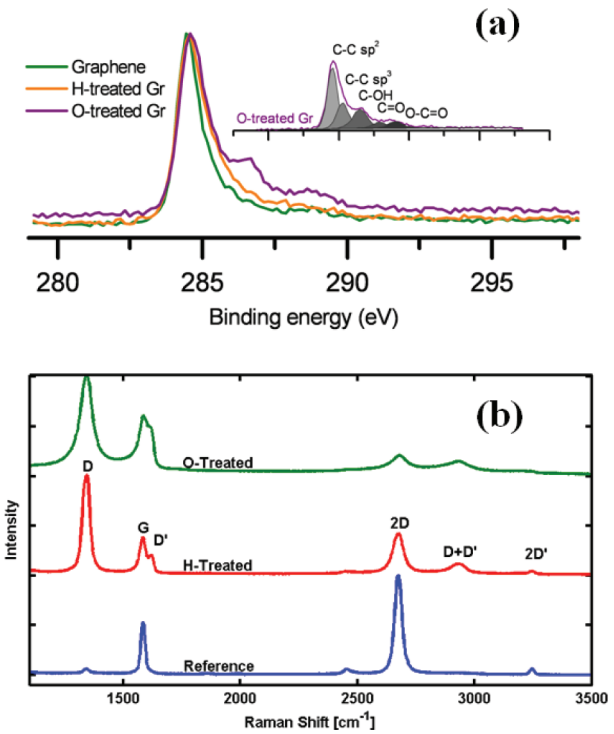

Figure 1. (a) High resolution C1s spectra of untreated graphene and plasma treated graphene. The inset shows the oxygen treated sample along with peak fitting results. (b) Averaged Raman spectra for each of the films analyzed in this study.

exposure to either the oxygen or hydrogen plasma. Such disorder is readily apparent in each film through the increased intensities of several spectral features (e.g., D, D′, and D + D′ modes) that are directly indicative of an alteration from an ideal graphene lattice. While both functionalized films do exhibit disorder, the extent of this disorder is substantially different. In the hydrogen exposed film for example, the 2D peak and the G-peak have much greater intensities than that of the D + D′ peak and the D′ peak, respectively. In contrast, the G and 2D features have similar intensities in comparison to the D′ and D + D′ modes for the film exposed to an oxygen plasma. In total, these results indicate increased disorder with either functionalization procedure albeit with a heightened disruption from exposure to the oxygen plasma relative to that of hydrogen.

The origin of this increased defect response can evolve from both plasma induced damage/amorphization of the graphene or changes in the carbon–carbon bonding structure that occur with covalent bonding of the oxygen/hydrogen onto the graphene lattice. Due to the low energy of the plasma functionalized procedure, no etching or changes in the lattice are expected to occur.[18,21] Therefore, we attribute the increased defect response of the Raman signal to result from the presence of the functionalized species (i.e., hydrogen/oxygen) rather than the inducement of any damage into the graphene lattice. Finally, it is of note that these changes do not alter the strain state[22] or carrier concentration[23] between the films as each are found to have peak positions of the G and 2D bands that are within the spectrometer resolution of ±1 cm^{-1}. Thus, any induced changes in the heat transport are a consequence of the bonding/defect states of the film and not due to strain or carrier effects.

Prior to TDTR measurements, we metalize each sample with 90 nm of electron beam evaporated Al at base pressures no

dx.doi.org/10.1021/nl203060j | Nano Lett. 2012, 12, 590–595

greater than 2.3×10^{-7} Torr. We then measure the thermal boundary conductance across the Al/SLG/SiO_2 interfaces with TDTR.[24] TDTR and appropriate analyses accounting for pulse accumulation when using a Ti:Sapphire oscillator have been discussed by several groups previously.[15,16,25−27] Our specific experimental setup is described in detail elsewhere.[16] In short, TDTR is a pump−probe technique in which our laser pulses emanate from a Spectra Physics Mai Tai with 90 fs pulses at 80 MHz repetition rate. We delay the time in which the probe pulse reaches the sample with respect to the pump pulse with a mechanical delay stage that gives ∼4 ns of probe delay. We modulate the pump path at 11 MHz and monitor the ratio of the in-phase to out-of-phase signal of the probe beam from a lock-in amplifier ($-V_{in}/V_{out}$). Our pump and probe spots are focused to 15 μm radii at the sample surface; at these sizes when modulating at 11 MHz, we should be negligibly sensitive to any in-plane transport in the graphene sheet[4,16] decreasing the uncertainty associated with determining h_K. We test each sample in a liquid nitrogen cooled cryostat and measure h_K from 100 to 400 K. We perform several TDTR scans at different locations of two different samples of each sample type (7−10 scans total for each type of graphene sample). Typical uncertainties due to the different locations on the samples or from sample to sample were less than 10% (calculated from the standard deviation among all the TDTR scans on a given sample type), which is smaller than the variation in metal/graphene/SiO_2 h_K expected due to a transition from SLG to n-layer graphene where $n > 1$ (∼25−35%), as measured via TDTR.[4] This further indicates that our samples were primarily SLG, confirming our Raman analysis. We fit the TDTR data with a model that accounts for pulse accumulation in a three-layer system (90 nm Al, 275 nm SiO_2, and Si). We adjust h_K between the Al and the SiO_2 to determine the Al/SLG/SiO_2 thermal boundary conductance.

Figure 2 shows the thermal boundary conductance of the various graphene samples as a function of temperature, T. There is a clear increase in the overall h_K of the Al/SLG/SiO_2 contact for the O-functionalized graphene, yet a slight decrease in h_K for the H-functionalized graphene as compared to the reference sample. At room temperature, we show an increase in h_K of ∼25% due to O-functionalization compared to the nonfunctionalized sample. As evident from the XPS and Raman analysis, both the H- and O-functionalization leads to increased sp^3 carbon bonds. In hydrogen, the C−H sp^3 bond is unreactive and thereby leaves the graphene surface inert.[28−30] However, it is well-known that the addition of oxygen functional groups on a surface greatly changes the surface energy, leading to an enhanced adhesion at a metal/oxide interface. This is mainly due to the oxide's electronic and structural properties. It was shown for example, that graphene oxide has a higher surface energy compared to graphene.[31] Moreover, in the C−O bond, one electron from the oxygen molecule is shared with the carbon, which, in turn leaves an additional electron to bond with the metal surface, thereby increasing the bond strength between the Al and the graphene. We also note that both the H-SLG and O-SLG exhibit disorder as compared to the nonfunctionalized SLG (c.f. Figure 1b). The effects of disorder on the cross plane thermal conductance of SLG are relatively minor and lead to a slight decrease, as determined by comparing the measured h_K at the Al/SLG/SiO_2 to the Al/H-SLG/SiO_2. Unlike our previous results in which we had shown reductions in h_K due to roughness at Al/Si interfaces,[32] the functionalization process in this work does not lead to a significant increase in the surface roughness of the graphene films. Therefore, we attribute the increase in h_K to the enhanced bonding in the Al/O-SLG/SiO_2.

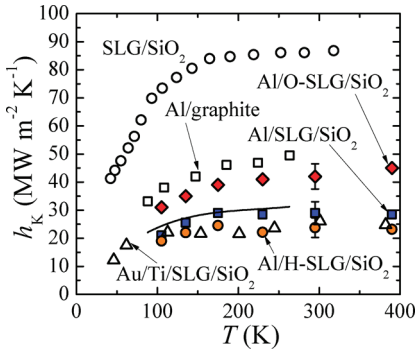

Figure 2. Measured thermal boundary conductances on the Al/SLG/SiO_2 sample (filled squares), the hydrogen functionalized sample (filled circles), and the oxygen functionalized sample (filled diamonds). The hydrogen functionalization process, which introduces disorder on the SLG, also leaves the SLG surface chemically inert and does not leave any additional bonding mechanism for the Al to the SLG. Functionalizing the SLG with oxygen leaves the graphene surface reactive leading to increased covalent bonds linking the Al to the SLG, which results in a higher phonon transmission and increase in h_K. For comparison, we also show h_K across SLG/SiO_2 (open circles, ref 10), Au/Ti/SLG/SiO_2 (open triangles, ref 4), and Al/graphite (open squares, ref 14) interfaces. Using these two measured conductances with eq 1, we can predict the Al/SLG/SiO_2 interface assuming that the Al/graphite h_K is similar to Al/SLG and that the Al/SLG and SLG/SiO_2 conductances can be separated. The resulting conductance, which is depicted by the solid line, is in very good agreement with our Al/SLG/SiO_2 measurements, indicating that the Al/SLG/SiO_2 thermal boundary conductance can be described by two separate conductances, Al/SLG and SLG/SiO_2.

For comparison, we also show h_K measured at a SLG/SiO_2 interface,[10] a Au/Ti/SLG/SiO_2 interface (the Ti is a 2 nm wetting layer),[4] and a Al/graphite interface.[14] Using these values for h_K at the Al/graphite and SLG/SiO_2 interface, we can compare our measured conductance across the Al/SLG/SiO_2 interface to an empirical prediction based on the assumption that the overall interface conductance can be separated into two conductances in series on either side of the graphene, given by

$$h_{K,metal/SLG/SiO_2} = \left(\frac{1}{h_{K,metal/SLG}} + \frac{1}{h_{K,SLG/SiO_2}} \right)^{-1} \quad (1)$$

This relation assumes that the cross plane thermal resistance of the SLG sheet is much less than the resistance at each of the interfaces, which is a valid assumption that has been addressed in detail previously.[4] eq 1 is shown in Figure 2 as the solid line, and shows relatively good agreement with our measured h_K across the Al/SLG/SiO_2 interface.

To directly compare the interface conductance between metals and SLG, we use eq 1 to estimate h_K across the metal/SLG interface by assuming that the SLG/SiO_2 thermal boundary conductance is the same as that measured by Chen et al.[10] and solving for $h_{k,metal/SLG}$ for the Al/SLG and Al/O-SLG interfaces in this work. These values for h_K at the Al/SLG and Al/O-SLG interfaces are shown in Figure 3 along with h_K Al/O-diamond (ref 33) Al/diamond interfaces (ref 34). We see a factor of 2 increase in h_K across the Al/O-SLG interface as

dx.doi.org/10.1021/nl203060j | Nano Lett. 2012, 12, 590−595

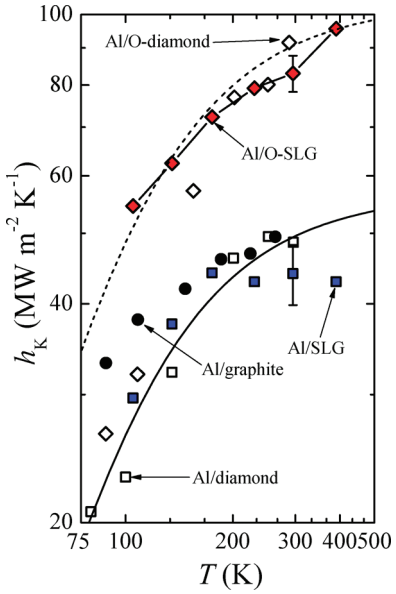

Figure 3. Thermal boundary conductance across our Al/SLG (filled squares) and Al/O-SLG (filled diamonds) interfaces derived from our experimental measurements across the Al/SLG/SiO_2 and Al/O-SLG/SiO_2 interface along with eq 1 and the data from the SLG/SiO_2 interfaces.[10] The thermal transport across the Al/SLG interface increases by a factor of 2 with oxygen functionalization of the graphene. Our derived values for h_K across the Al/SLG interface are in good agreement with conductances measured across Al/graphite (filled circles, ref 14) and Al/diamond interfaces (open squares, ref 34). Similarly, our derived values for Al/O-SLG h_K is in good agreement with Al/O-diamond measurements (open diamonds, ref 33). We model the thermal conductance across the Al/SLG interface with the DMM (eqs 2−5), as shown by the solid line. We adjust the velocity of the SLG in our DMM calculations to model the Al/O-SLG thermal boundary conductance (dashed line), and find that the resultant velocity in the oxygenated SLG is about a factor of 2 higher than the nonfunctionalized sample. This is indicative of the increase in bond strength between the Al and the SLG via the oxygen adsorbates.

compared with the Al/SLG interface. We attribute this observed behavior to the enhanced reactivity of the oxygenated surface, which is consistent with the increase observed across the Al/O-diamond interface as compared to the Al/diamond interface. Recall that the presence of oxygen-containing functional groups increases the surface energy and thus makes graphene more reactive, allowing a lower energy bonding state with the evaporated Al film as compared to the untreated SLG which is chemically inert.[28−30] This lower energy bonding state promotes Al−O formation, leading to a stronger Al−O−SLG junction and thereby an increase in h_K. Still, it is interesting that while hydrogen-termination can significantly decrease the conductance of Al/diamond interfaces,[33] it has minimal effect on Al/graphene interfaces (see Figure 2).

To quantify this, we turn to the diffuse mismatch model (DMM).[8] Assuming crystallographic isotropy in the Al film, the thermal boundary conductance from the Al to the SLG is given by

$$h_K = \frac{1}{8\pi^2}\sum_j \int_{k_1} \hbar\omega_j(k)k^2\frac{\partial f}{\partial T}v_{1,j}(k)\zeta_{1\to 2}\,\mathrm{d}k \tag{2}$$

where $\hbar$ is the reduced Planck's constant, ω is the phonon angular frequency, k is the phonon wavevector, f is the Bose−Einstein distribution function, T is the temperature, v is the velocity, and ζ is the phonon transmission coefficient from side 1 to side 2 (which ranges from 0 to 1). Here, the subscript "1" refers to the corresponding property of Al, "2" refers to the corresponding property of graphene, and j refers to the phonon polarization. To calculate the transmission coefficient, we use the assumption discussed by Duda et al.[35] in which we treat the graphene sheet as a two-dimensional solid. Therefore, performing detailed balance on the fluxes in the Al and SLG,[36] we obtain

$$\zeta_{1\to 2} = \frac{q_2}{q_1 + q_2} \tag{3}$$

where q is the phonon flux. For the flux in the Al, we can make the usual approximation of phonon flux,[37] which is the basis of the derivation of eq 2,[38] namely

$$q_1 = \frac{1}{8\pi^2}\sum_j \int_{k_1} \hbar\omega_j(k)k^2 f v_{1,j}(k)\zeta_{1\to 2}\,\mathrm{d}k \tag{4}$$

However, given the two-dimensional nature of the SLG, the phonon flux in this material is given by[35]

$$q_2 = \frac{1}{8\pi a}\sum_j \int_{k_2} \hbar\omega_j(k)k f v_{2,j}(k)\,\mathrm{d}k \tag{5}$$

where a is the interlayer spacing of graphite (i.e., a = 3.35 Å).[39] For calculations of eqs 2−5, we fit polynomials to the phonon dispersions of Al in the Γ→X direction[40] and of graphene in the Γ → K direction[41] to give greater accuracy in the DMM calculations as compared to the Debye approximation.[42] We note, however, that the modes in the Γ → K in graphene are extremely Debye-like (i.e., non dispersive) in the frequency regime that is elastically accessible to the Al (frequencies below 10 THz). We ignore the ZA mode in the graphene dispersion since the ZA mode is heavily suppressed in encased and supported SLG.[7,43] We note that our calculations in eq 3 are balancing the total flux, and not the flux at any given frequency. We assume elastic scattering in this calculation. Therefore, we restrict the wavevector in each mode of the SLG and perform the integration only to the wavevector of the corresponding mode. As a result, no frequencies above the cutoff frequency of Al can participate in h_K. Also, given that our measurements represent the cross plane conductance of Al/SLG, the cross plane velocity of SLG is meaningless. Therefore, we define $v_{2,j}$ as a fitting parameter that we assume is constant with wavevector. This is a similar approach as performed in the analysis of Koh et al.[4] in which they adjust q_2 to fit the DMM to their Au/Ti/SLG data and Schmidt et al. in which they adjust the phonon transmission to fit the DMM to their metal/graphite data.[14] We note that this approach of adjusting only $v_{2,j}$ gives us more direct insight into how the bonding at the Al/SLG interface changes due to the functionalization since we are not adjusting any aspect of the graphene dispersion, only the transport velocity. The fits of DMM are shown in Figure 3. The solid line is the DMM calculation assuming that the graphene cross plane velocities are $v_{2,L}$ = 2,455 m/s and $v_{2,T}$ = 1,480 m/s for the longitudinal and transverse modes of the SLG, respectively. The dashed line is the DMM calculations assuming $v_{2,L}$ = 4,687 m/s and $v_{2,T}$ = 2,825 m/s for the longitudinal and transverse modes of the O-SLG, respectively. The velocities that result in the best fit of the DMM to the SLG data are in good agreement with the cross plane velocity of bulk

dx.doi.org/10.1021/nl203060j | Nano Lett. 2012, 12, 590−595

graphite,[39] which could be indicative of similar bonding between the Al and SLG as the van der Waals bonds cross plane in graphite. The velocities resulting in the best fit in the Al/O-SLG data are nearly a factor of 2 higher, which we attribute to the increased bond strength between the Al and SLG due to the presence of oxygen leading to covalent bonding with the Al and O-SLG. It is important to note that we use the velocity parameter and fitting only to lend insight into the nature of the bonding at the two different interfaces. Since the velocity is proportional to the square root of the spring constant, the increase by a factor of 2 in the best-fit velocity with oxygen functionalization implies that increase in thermal transport is due to an increase in interfacial bond strength by roughly 40%.

We cannot preclude the possibility that the change in electron population from the functionalization could be affecting the measured thermal boundary conductance. However, Majumdar and Reddy[44] showed that electron−phonon coupling could decrease the thermal boundary conductance, an opposite trend as what is observed in our O-SLG interfaces. In addition, they concluded that the electron−phonon resistance only contributes to interfacial transport when the phonon-mediated conductance is on the order of $GW/m^2/K$, which is over an order of magnitude greater than the values we report here for the thermal boundary conductance at our graphene interfaces. Lyeo and Cahill[45] experimentally determined that electron scattering does not affect thermal transport across metal/diamond interfaces. The covalent nature of the diamond bond in their study suggests that the oxygen functionalization of our graphene should not add any additional thermal mechanisms via the electrons. Finally, Hopkins et al.[46,47] demonstrated that an increase in thermal boundary conductance due to electron transport will only occur during regimes of electron−phonon nonequilibrium; our TDTR measurements are conducted during time delays that are orders of magnitudes greater than typical electron−phonon nonequilibrium regimes. Collectively, this alludes to the fact that the increase in thermal boundary conductance due to oxygen functionalization is due to changes in the nature of the chemical bond at the Al/graphene interface, and not due to any change in electronic contribution.

The data in Figures 2 and 3 also give insight into the fundamental phonon mechanisms involved with thermal boundary conductance across Al and carbon-based materials. For example, without any chemical functionalization, Al/graphene, Al/graphite, and Al/diamond all show similar values for thermal boundary conductance despite the fact these three carbon-based materials all have different dispersion relations. At Al/graphene and Al/diamond interfaces, oxygenation leads to a significant increase in thermal boundary conductance. This suggests that conductance at these interfaces is otherwise limited by interfacial bond strength. For comparison, we plot the ratio of our Al/O-SLG data to our Al/SLG data (Al/O-SLG:Al/SLG) along with the ratio the Al/O-diamond to Al/diamond (Al/O-diamond:Al/diamond), shown in Figure 4. These ratios are very similar, especially at elevated temperatures, which would be indicative of a similar increase in the force constants at the Al−O bond compared to the Al-graphene or Al-diamond bond. Also in this figure, we plot the ratio of h_K across a Au/(2 nm)Ti/SLG interface[5] (calculated via eq 1) to h_K across an Au/graphite interface.[14] Presumably, the Ti wetting layer between the Au and SLG should increase the wettability of the Au to the SLG. However, the two

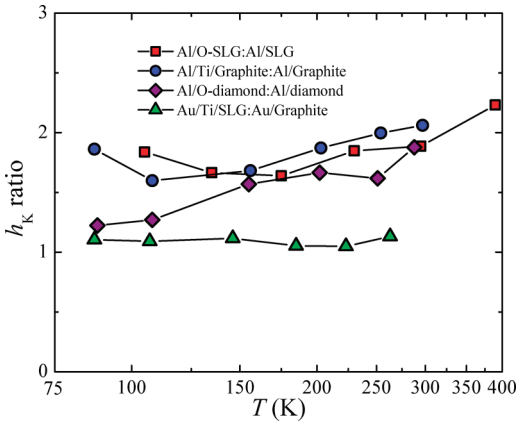

Figure 4. Ratio of thermal boundary conductance Al/O-SLG to Al/SLG (filled squares). For comparison, we also plot the ratio of h_K across the Al/O-diamond interface[33] to the Al/diamond interface[34] (filled diamonds). We also plot the ratio of h_K across the Al/Ti/Graphite to the Al/Graphite interfacial conductance (filled circles). These ratios are very similar, especially at elevated temperatures, which would be indicative of a similar increase in the elastic constants at the Al−O bond compared to the Al-graphene or Al-diamond bond. We plot the ratio of h_K across a Au/(2 nm)Ti/SLG interface to h_K across an Au/graphite interface[14] (filled triangles). The two conductances are nearly identical over the entire temperature range (i.e., Au/(2 nm)Ti/SLG:Au/graphite ∼1). Where the Ti will increase the adhesion, Au is a very soft material with low phonon velocities and weak elastic constants. Therefore, the phonon flux in gold is so low that regardless of the strength of the bond at the Au/SLG or graphite interfaces, the phonon transmissivity will always be limited by the phonon flux in the Au.

conductances are nearly identical over the entire temperature range (i.e., Au/(2 nm)Ti/SLG:Au/graphite ∼1). On the contrary, conductances at Al:(5 nm)Ti/graphite interfaces are approximately a factor of 2 higher than those at Al/graphite interfaces 80 to 300 K. While Ti layers increase adhesion strength at metal/graphite interfaces, the increased adhesion only benefits the Al/carbon interfaces. This makes intuitive sense, as the phonon frequencies are much lower in Au than Ti, and thus, are less affected by a weakly bonded interface. While both chemical-functionalization and the inclusion of an adhesion layer can increase the conductance at Al/carbon interfaces, chemical functionalization does not require the inclusion of additional materials, nor does it increase the relative "thickness" of the interface (e.g., 5 nm of Ti corresponds roughly to the thickness of 15 layers of graphene). Regardless, the interplay between the efficiency of thermal transport and the bond strength at the metal/SLG interface has major implications for engineering and development of graphene-based devices in which contact resistances plague the device performance.

In summary, we have investigated the effects of functionalization on the thermal boundary conductance across metal/graphene interfaces through the introduction of chemical adsorbates on the SLG surfaces in order to increase the density of covalent bonds bridging the metal and the SLG. Specifically, we metalized plasma-functionalized graphene and measured h_K at Al/SLG/SiO_2 contacts with time domain thermoreflectance. Through these measurements, adsorbates on the SLG surfaces were shown to influence the cross plane thermal conductance. These influences are attributed to changes in bonding between the metal and the SLG. The

dx.doi.org/10.1021/nl203060j | Nano Lett. 2012, 12, 590−595

thermal boundary conductance was found to be most influenced by the interfacial chemical bonding as both the phonon flux and the vibrational mismatch between the materials are each subject to the to the interfacial bond strength. In the case of oxygen functionalization, we show that the thermal boundary conductance increases, which is attributed to the increase in the chemical bond strength at the Al/SLG interface. The fact that oxygen functionalization leads to an increase in thermal transport demonstrates the powerful role of chemical bonding on thermal transport across graphene interfaces.

AUTHOR INFORMATION

Corresponding Author

*E-mail: phopkins@virginia.edu; scott.walton@nrl.navy.mil.

ACKNOWLEDGMENTS

P.E.H. is grateful for funding from the National Science Foundation (CBET-1134311). P.E.H., T.E.B., and J.C.D. gratefully acknowledge support from the LDRD Program through Sandia National Laboratories. M.B. appreciates the support of the National Research Council. This work was partially supported by the Office of Naval Research. J.C.D. gratefully acknowledges support from the National Science Foundation through the Graduate Research Fellowship Program. This work was performed, in part, at the Center for Integrated Nanotechnologies, a U.S. Department of Energy, Office of Basic Energy Sciences user facility. Sandia National Laboratories is a multiprogram laboratory managed and operated by Sandia Corporation, a wholly owned subsidiary of Lockheed Martin Corporation, for the U.S. Department of Energy's National Nuclear Security Administration under Contract DE-AC04-94AL85000.

REFERENCES

(1) Castro Neto, A. H.; Guinea, F.; Peres, N. M. R.; Novoselov, K. S.; Geim, A. K. *Rev. Mod. Phys.* **2009**, *81*, 109−162.

(2) Peres, N. M. R. *Rev. Mod. Phys.* **2010**, *82*, 2673−2700.

(3) Balandin, A. A.; Ghosh, S.; Bao, W.; Calizo, I.; Teweldebrhan, D.; Miao, F.; Lau, C. N. *Nano Lett.* **2008**, *8*, 902−907.

(4) Koh, Y. K.; Bae, M.-K.; Cahill, D. G.; Pop, E. *Nano Lett.* **2010**, *10*, 4363−4368.

(5) Wang, Z.; Xie, R.; Bui, C. T.; Liu, D.; Ni, X.; Li, B.; Thong, J. T. L. *Nano Lett.* **2011**, *11*, 113−118.

(6) Ghosh, S.; Bao, W.; Nika, D. L.; Subrina, S.; Pokatilov, E. P.; Lau, C. N.; Balandin, A. A. *Nat. Mater.* **2010**, *9*, 555−558.

(7) Seol, J. H.; Jo, I.; Moore, A. L.; Lindsay, L.; Aitken, Z. H.; Pettes, M. T.; Li, X.; Yao, Z.; Huang, R.; Broido, D. A.; Mingo, N.; Ruoff, R. S.; Shi, L. *Science* **2010**, *328*, 213−216.

(8) Swartz, E. T.; Pohl, R. O. *Rev. Mod. Phys.* **1989**, *61*, 605−668.

(9) Kapitza, P. L. *Zhurnal Eksperimentalnoi I Teoreticheskoi Fiziki* **1941**, *11*, 1−31.

(10) Chen, Z.; Jang, W.; Bao, W.; Lau, C. N.; Dames, C. *Appl. Phys. Lett.* **2009**, *95*, 161910.

(11) Norris, P. M.; Hopkins, P. E. *J. Heat Transfer* **2009**, *131*, 043207.

(12) Cai, W.; Moore, A. L.; Zhu, Y.; Li, X.; Chen, S.; Shi, L.; Ruoff, R. S. *Nano Lett.* **2010**, *10*, 1645−1651.

(13) Swartz, E. T.; Pohl, R. O. *Rev. Mod. Phys.* **1989**, *61*, 605−665.

(14) Schmidt, A. J.; Collins, K. C.; Minnich, A. J.; Chen, G. *J. Appl. Phys.* **2010**, *107*, 104907.

(15) Cahill, D. G. *Rev. Sci. Instrum.* **2004**, *75*, 5119−5122.

(16) Hopkins, P. E.; Serrano, J. R.; Phinney, L. M.; Kearney, S. P.; Grasser, T. W.; Harris, C. T. *J. Heat Transfer* **2010**, *132*, 081302.

(17) Li, X.; Cai, W.; An, J.; Kim, S.; Nah, J.; Yang, D.; Piner, R.; Velamakanni, A.; Jung, I.; Tutuc, E.; Banerjee, S. K.; Colombo, L.; Ruoff, R. S. *Science* **2009**, *324*, 1312−1314.

(18) Baraket, M.; Walton, S. G.; Lock, E. H.; Robinson, J. T.; Perkins, F. K. *Appl. Phys. Lett.* **2010**, *96*, 231501.

(19) Walton, S. G.; Muratore, C.; Leonhardt, D.; Fernsler, R. F.; Blackwell, D. D.; Meger, R. A. *Surf. Coat. Technol.* **2004**, *186*, 40−46.

(20) Ferrari, A. C.; Meyer, J. C.; Scardaci, V.; Casiraghi, C.; Lazzeri, M.; Mauri, F.; Piscanec, S.; Jiang, D.; Novoselov, K. S.; Roth, S.; Geim, A. K. *Phys. Rev. B* **2006**, *97*, 187401.

(21) Nourbakhsh, A.; Cantoro, M.; Vosch, T.; Pourtois, G.; Clemente, F.; van der Veen, M. H.; Hofkens, J.; Heyns, M. M.; De Gendt, S.; Sels, B. F. *Nanotechnology* **2010**, *21*, 435203.

(22) Mohiuddin, T. M. G.; Lombardo, A.; Nair, R. R.; Bonetti, A.; Savini, G.; Jalil, R.; Bonini, N.; Basko, D. M.; Galiotis, C.; Marzari, N.; Novoselov, K. S.; Geim, A. K.; Ferrari, A. C. *Phys. Rev. B* **2009**, *79*, 205433.

(23) Das, A.; Chakraborty, B.; Piscanec, S.; Pisana, S.; Sood, A. K.; Ferrari, A. C. *Phys. Rev. B* **2009**, *79*, 155417.

(24) Cahill, D. G.; Goodson, K. E.; Majumdar, A. *J. Heat Transfer* **2002**, *124*, 223−241.

(25) Schmidt, A.; Chiesa, M.; Chen, X.; Chen, G. *Rev. Sci. Instrum.* **2008**, *79*, 064902.

(26) Schmidt, A. J.; Chen, X.; Chen, G. *Rev. Sci. Instrum.* **2008**, *79*, 114902.

(27) Hopkins, P. E.; Kaehr, B.; Phinney, L. M.; Koehler, T. P.; Grillet, A. M.; Dunphy, D.; Garcia, F.; Brinker, C. J. *J. Heat Transfer* **2011**, *133*, 061601.

(28) Lee, B.; Park, S.-Y.; Kim, H.-C.; Cho, K.; Vogel, E. M.; Kim, M. J.; Wallace, R. M.; Kim, J. *Appl. Phys. Lett.* **2008**, *92*, 203102.

(29) Wang, H.; Griffiths, J.-P.; Egdell, R. G.; Moloney, M. G.; Foord, J. S. *Langmuir* **2008**, *24*, 862−868.

(30) Kim, J.; Kim, T. W. *JOM* **2009**, *61*, 17−22.

(31) Walton, S. G.; Lock, E. H.; Baraket, M.; Sheehan, P. E.; Wei, Z.; Robinson, J. T. Snow, E. S. *Proceedings of the Society of Vacuum Coaters* 2009, *52nd Annual Technical Conference*, 525−528.

(32) Hopkins, P. E.; Phinney, L. M.; Serrano, J. R.; Beechem, T. E. *Phys. Rev. B* **2010**, *82*, 085307.

(33) Collins, K. C.; Chen, G. *Appl. Phys. Lett.* **2010**, *97*, 083102.

(34) Stoner, R. J.; Maris, H. J.; Anthony, T. R.; Banholzer, W. F. *Phys. Rev. Lett.* **1992**, *68*, 1563−1566.

(35) Duda, J. C.; Smoyer, J. L.; Norris, P. M.; Hopkins, P. E. *Appl. Phys. Lett.* **2009**, *95*, 031912.

(36) Vincenti, W. G. Kruger, C. H. *Introduction to Physical Gas Dynamics*; Krieger Publishing Company: Malabar, FL, 2002.

(37) Chen, G. *Nanoscale Energy Transport and Conversion: A Parallel Treatment of Electrons, Molecules, Phonons, and Photons*; Oxford University Press: New York, 2005.

(38) Duda, J. C.; Hopkins, P. E.; Smoyer, J. L.; Bauer, M. L.; English, T. S.; Saltonstall, C. B.; Norris, P. M. *Nanoscale Microscale Thermophys. Eng.* **2010**, *14*, 21−33.

(39) Nicklow, R.; Wakabayashi, N.; Smith, H. G. *Phys. Rev. B* **1972**, *5*, 4951−4962.

(40) Gilat, G.; Nicklow, R. M. *Phys. Rev.* **1966**, *143*, 487−494.

(41) Viola Kusminskiy, S.; Campbell, D. K.; Castro Neto, A. H. *Phys. Rev. B* **2009**, *80*, 035401.

(42) Duda, J. C.; Beechem, T.; Smoyer, J. L.; Norris, P. M.; Hopkins, P. E. *J. Appl. Phys.* **2010**, *108*, 073515.

(43) Jang, W.; Chen, Z.; Bao, W.; Lau, C. N.; Dames, C. *Nano Lett.* **2010**, *10*, 3909−3913.

(44) Majumdar, A.; Reddy, P. *Appl. Phys. Lett.* **2004**, *84*, 4768−4770.

(45) Lyeo, H.-K.; Cahill, D. G. *Phys. Rev. B* **2006**, *73*, 144301.

(46) Hopkins, P. E.; Kassebaum, J. L.; Norris, P. M. *J. Appl. Phys.* **2009**, *105*, 023710.

(47) Hopkins, P. E.; Norris, P. M. *Appl. Surf. Sci.* **2007**, *253*, 6289−6294.